Scientific Reports

https://doi.org/10.1038/s41598-026-41706-w

Article in Press

Percolation threshold for vertical fluid flow through granular sea ice

Received: 5 September 2025

Accepted: 23 February 2026

Published online: 28 February 2026

Cite this article as: Golden K.M., Furse C.M., Gully A. *et al.* Percolation threshold for vertical fluid flow through granular sea ice. *Sci Rep* (2026). https://doi.org/10.1038/s41598-026-41706-w

Kenneth M. Golden, Cynthia M. Furse, Adam Gully, Joyce Lin, Delaney Q. Mosier, Christian Sampson & Jean-Louis Tison

Percolation threshold for vertical fluid flow through granular sea ice

Kenneth M. Golden[1], Cynthia M. Furse[2], Adam Gully[1], Joyce Lin[3], Delaney Q. Mosier[1], Christian Sampson[4], and Jean-Louis Tison[5]

[1]University of Utah, Department of Mathematics
155 S 1400 E RM 233, Salt Lake City, UT 84112-0090 USA

[2]University of Utah, Department of Electrical and Computer Engineering
50 S Central Campus Drive RM 2110 MEB, Salt Lake City, UT 84112 USA

[3]Department of Mathematics, California Polytechnic State University
San Luis Obispo, CA 93407-0403 USA

[4]Joint Center For Satellite Data Assimilation, UCAR
Foothills Lab 4, 3300 Mitchell Lane, Boulder, CO 80301 USA

[5]DSTE, Laboratoire de Glaciologie, CP 160/03, Université Libre de Bruxelles
50, av. F. D. Roosevelt, 1050 Bruxelles, Belgium

[Corresponding author, Kenneth M. Golden, email: ken.golden@utah.edu]

Abstract

The fluid permeability of sea ice governs a broad range of physical and biological processes in the polar marine environment, such as melt pond evolution, snow-ice formation, and nutrient replenishment for sea ice algae. Columnar sea ice is effectively impermeable to bulk flow for brine volume fractions below about 5%, while above this threshold fluid can flow vertically through the ice. Granular sea ice has different crystallographic and brine microstructures. It has long formed a significant portion of the Antarctic sea ice cover, and has become increasingly prevalent in the rapidly changing Arctic. Data gathered off the coast of East Antarctica indicate that this threshold for bulk vertical flow through granular sea ice there is around 10%. While columnar and granular microstructures display quite different threshold values, percolation theory predicts that they have the same universal critical exponent for the permeability as a function of porosity above the threshold, which agrees closely with our data. These findings impact physical and ecological modeling efforts, and must be taken into account when granular ice is present.

1 Introduction

The Arctic and Antarctic sea ice covers form a critical component of Earth's surface layer, significantly impacting planetary albedo, and regulate the exchange of heat, gases, and momentum between the ocean and atmosphere in the polar regions [1, 2]. They also play a crucial role in polar marine ecosystems, hosting life from microbes like algae and bacteria, to penguins and polar bears [1, 3]. The polar sea ice covers are also sensitive indicators of planetary warming. Arctic sea ice decline over the satellite era has been dramatic and consequential, with rapidly decreasing extent, a younger, thinner sea ice cover, and longer melt seasons [4, 5, 6]. Antarctic sea ice has recently seen record lows, with some evidence of a regime shift [7, 8].

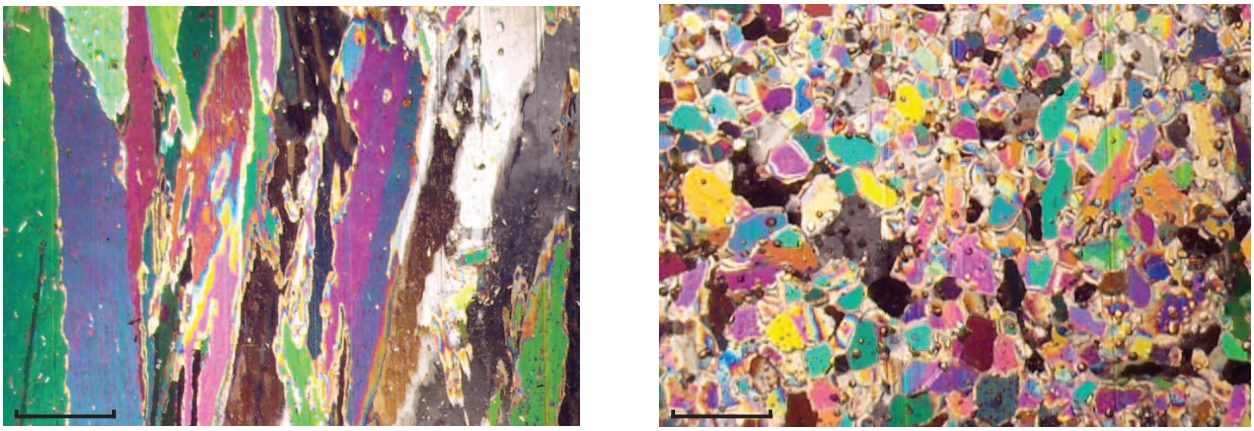

Figure 1: An image of the polycrystalline microstructure of Antarctic columnar ice under cross-polarization is shown on the left, and an image of granular ice is shown on the right. These samples were taken in the Bellingshausen Sea in October 2007 during the Sea Ice Mass Balance in the Antarctic (SIMBA) experiment [30]. The horizontal scale of each image is 6.1 cm, while the scale bars each represent 1 cm.

Given the geophysical and ecological significance of sea ice and the substantial changes observed recently, accurate representation of sea ice and its key physical and biological processes is critical to improving large-scale predictive models [9, 10]. As a material, sea ice is a multiscale composite with complex structure on length scales ranging over many orders of magnitude. Of central importance to the material properties of sea ice are its centimeter-scale polycrystalline microstructure, and the millimeter-scale brine inclusion microstructure [2, 11, 12, 13]. In columnar ice individual crystals typically contain layers of brine inclusions, and in granular ice the brine tends to reside within the interstices between small ice grains, as shown in Figure 1. In particular, we focus here on one crucial property which impacts both sea ice physics and biology: fluid permeability.

Fluid flow through the porous microstructure of sea ice regulates melt pond evolution affecting ice pack albedo [14, 15], brine drainage and the evolution of salinity profiles [11, 2], snow-ice formation, where sea water floods the ice surface and then freezes [16, 17], ocean-ice-atmosphere exchanges of gases such as CO_2, CH_4, DMS, and N_2O [18, 19, 20], convection-enhanced thermal transport [21, 22, 23], and biomass build-up fueled by nutrient fluxes [24, 25, 1]. Fluid flow also serves as the mechanism for the nutrient replenishment necessary to sustain the algal and bacterial communities living within the ice [26].

The fluid permeability of sea ice plays a significant role in understanding the processes described above, and in parameterizing them in large-scale models. Previously it was found that for brine volume fractions ϕ below approximately 5%, columnar sea ice is effectively impermeable to fluid flow, but is permeable for ϕ above 5% [27, 28]. For a typical bulk salinity of 5 parts per thousand (ppt), this critical porosity $\phi_c \approx 5\%$ corresponds [29, 2, 11] to a critical temperature $T_c \approx -5°\mathrm{C}$, which has been widely used in sea ice modeling [28, 10] and is known as the *rule of fives*.

It was predicted [27], however, that granular sea ice, with a more random distribution of brine inclusions, would exhibit a higher critical brine volume fraction required for bulk fluid flow. This prediction was in close alignment with Antarctic field data on snow-ice formation and a convection-driven algal bloom [25]. Recently, in [31], key differences were found in the vertical tortuosities and correlation lengths of the pore spaces between granular and columnar ice, with the brine in granular ice less interconnected. They utilized X-ray CT data and the Kozeny-Carman relation to conclude

that granular ice has lower permeability than columnar ice. They did not, however, estimate a percolation threshold due to spread in the microstructural data and noted that "ultimately, permeability measurements of granular ice are required."

Here we present a comprehensive set of bail test measurements of the fluid permeability of granular sea ice taken off the coast of East Antarctica during the SIPEX II expedition, September - November 2012 [32]. We find that the critical threshold ϕ_c for bulk fluid flow in the vertical direction is about 10%, and that predictions from percolation theory for the fluid permeability as a function of brine porosity ϕ [33, 34, 28, 12] agree closely with our data.

We emphasize that our principal conclusion of the 10% critical threshold for Antarctic granular ice is based primarily on the results of the carefully conducted bail test measurements. However, this value of about 10% is also predicted here through a simple analysis of photomicrographs of Antarctic granular ice, which yields values for the geometrical parameters in a model of compressed powders [35, 36, 37] that was used in [27] to predict the 5% threshold for columnar ice. While the compressed powder model is an overly simplified representation of sea ice microstructure, it still provides a useful way of understanding why the critical porosity for granular ice is significantly higher than for columnar ice. Interestingly, the compressed powder model was introduced in the development of radar absorbing materials [38] used to coat aircraft and ships, making them *stealthy* and difficult to detect.

In addition to the above microstructural analysis used in the compressed powder model to support the finding of the 10% threshold for Antarctic granular ice, we also present here results from the SIPEX I voyage [39] during September and October of 2007. Golden & Gully conducted tracer experiments on blocks of sea ice collected off the coast of East Antarctica. The results show a sharp transition in fluid flow properties at depths corresponding to 10% porosity. They indirectly support our direct findings from the bail test experiments that granular sea ice is effectively impermeable to bulk vertical flow for brine porosities below about 10%. However, these tracer experiments were more exploratory in nature, and were not specifically designed to find the percolation threshold, but to observe brine channels and fluid flow in Antarctic sea ice. It was only after analyzing brine volume fraction profiles and crystallographic observations that we realized that these dye experiments might also provide supporting evidence for the 10% threshold.

Percolation theory [33, 34] gives predictions for the vertical fluid permeability of granular sea ice for porosities above the observed percolation threshold of 10%. In particular, the theory predicts power law behavior for the permeability in this regime with a critical exponent describing its behavior. Interestingly, it was shown [28, 12] that this exponent for columnar sea ice − a complex porous medium in the continuum, takes the same universal value that holds for lattice percolation models. The recent results in [31] on the characteristics of the brine inclusions in granular sea ice enable us to find here that the critical exponent describing the permeability above the 10% threshold in granular ice takes this same universal lattice value as for columnar sea ice, which is in very close agreement with our data.

Finally, we note that for many reasons columnar microstructures have received disproportionate attention, mostly due to their prevalence in Arctic sea ice and their importance in undisturbed ice growth [11, 40, 2], while granular microstructures have historically received less focus. However, granular ice is common in surface layers in the Arctic [41, 42], which directly underlie ponds controlling ice albedo. This becomes particularly important as we observe a regime shift toward younger, thinner Arctic sea ice [43]. Examination of the crystalline structure in sea ice from a more recent trans-Arctic survey showed a marked increase in overall granular ice fraction, from around 10% observed in an earlier study [44] to over 40% [42]. In the Antarctic it has long been observed that granular ice [45, 16, 46] accounts for up to 40% of the sea ice pack. Snow-ice in particular, with a granular microstructure itself, accounts for over a quarter of the ice found in the Southern

Ocean [47], and there has been recent interest in assessing changing conditions in the Arctic that may promote snow-ice formation there [17]. An accurate accounting of sea ice processes involving fluid flow in predictive geophysical, biological, and biogeochemical models in either the Arctic or Antarctic thus relies on a deeper knowledge of the fluid permeability of granular ice.

2 Results

Field Experiments

During September and October of 2012, we measured the fluid permeability of first year Antarctic pack ice as participants in SIPEX II aboard the ice breaker *Aurora Australis* off the east coast of Antarctica [32]. Over 100 measurements of the fluid permeability of the ice were made covering a range of depths, temperatures, and ice types [48] (see Methods). Brine volume fraction profiles for full and partial cores were obtained from temperature and salinity data for 10 cm sections of the cores using the Frankenstein-Garner relation [29, 2, 11]. Full crystallographic cores were taken at each site in order to correlate ice type to specific permeability measurements, and the measurements corresponding to granular ice were separated out. We found that the critical threshold for fluid flow in granular ice was around $\phi_c \approx 10\%$. For a typical salinity of approximately 5 ppt, the corresponding critical temperature is around $T_c \approx -2.5°\mathrm{C}$ [29]. Moreover as predicted by the percolation theory analysis initiated in [28], we find here that the *universal* lattice critical exponent of about 2 for columnar ice in the Arctic still accurately describes the take-off of $k(\phi)$ above the threshold $\phi_c \approx 0.1$ for the granular case, as shown in Figure 2.

In September and October of 2007, during the SIPEX I voyage [39], we conducted tracer experiments on sea ice samples collected off the coast of East Antarctica. The tracer experiments consisted of extracting blocks of sea ice with a chainsaw, turning them upside down, and pouring cooled water with food dye or fluorescein (and some salt so that the fluid was similar in salinity and temperature to sea water) into shallow channels cut into the bottom of the ice (which was the top surface of the inverted blocks). Thin vertical slices were then cut from the blocks to expose the fluid fronts and layers of different microstructures and brine channels. In each iteration of the experiment, the fluid descended within a couple minutes through a layer of highly permeable sea ice, and stopped when it reached colder, impermeable granular ice (or fine-grained columnar ice) of brine volume fraction around 10%, as shown in Figure 3. The brine volume fraction profile of the blocks was determined by depth-matching to an adjacent ice core whose brine porosity profile was again determined using the Frankenstein-Garner relation [29, 1, 2]. The required temperature profile for this core was taken immediately upon extraction, with salinity determined from melted 10 cm sections later on the ship. The ice type was determined, as best could be discerned, from visual inspection of the large thin slices, and comparison with other cores at that ice station, where the ice field there was quite homogeneous.

These experiments, as well as the above findings on fluid permeability and the compressed powder model, vividly illustrate that the critical threshold for fluid transport in fine-grained sea ice can be much higher than the 5% brine volume fraction for classic columnar sea ice, like that shown on the left in Figure 1. We note, however, as mentioned above, the tracer experiments were originally quite exploratory. They were conducted to obtain observations through photos and video of fluids moving through sea ice. After seeing our permeability results for SIPEX II, though, we realized that the observations of tracers in SIPEX I, when combined with analysis of brine volume profiles, could shed light on the threshold question for granular ice.

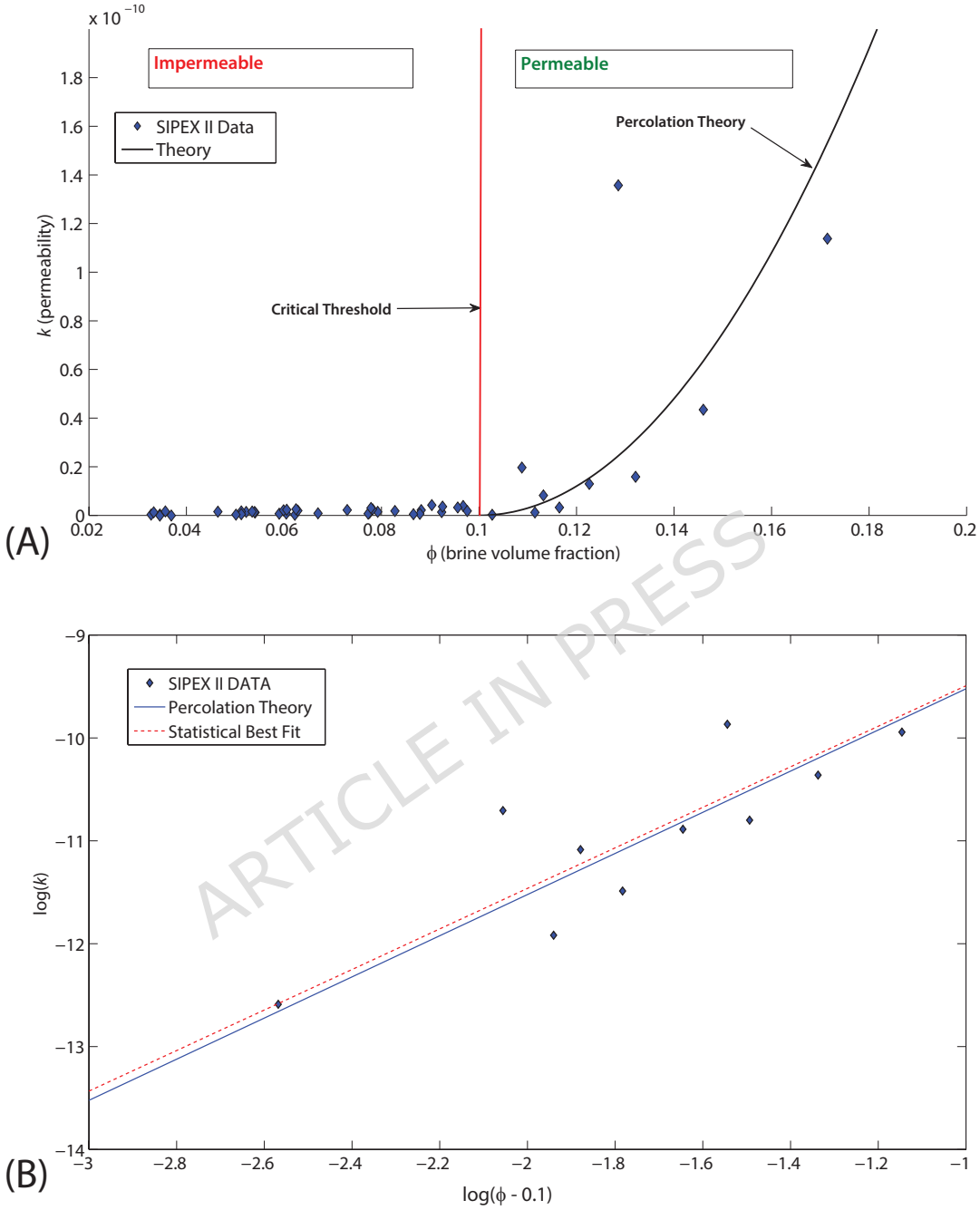

Figure 2: Comparison of *in situ* data on k (m^2) for Antarctic sea ice with percolation theory. In **(A)** all the granular sea ice data are displayed on a linear scale and in **(B)** the granular data for porosities above 10% are shown on a logarithmic scale, relative to $\phi_c \approx 0.1$, where a statistical best fit (dotted red line) of the data is shown along with the percolation theory prediction (solid blue line) with $\phi_c \approx 0.1$.

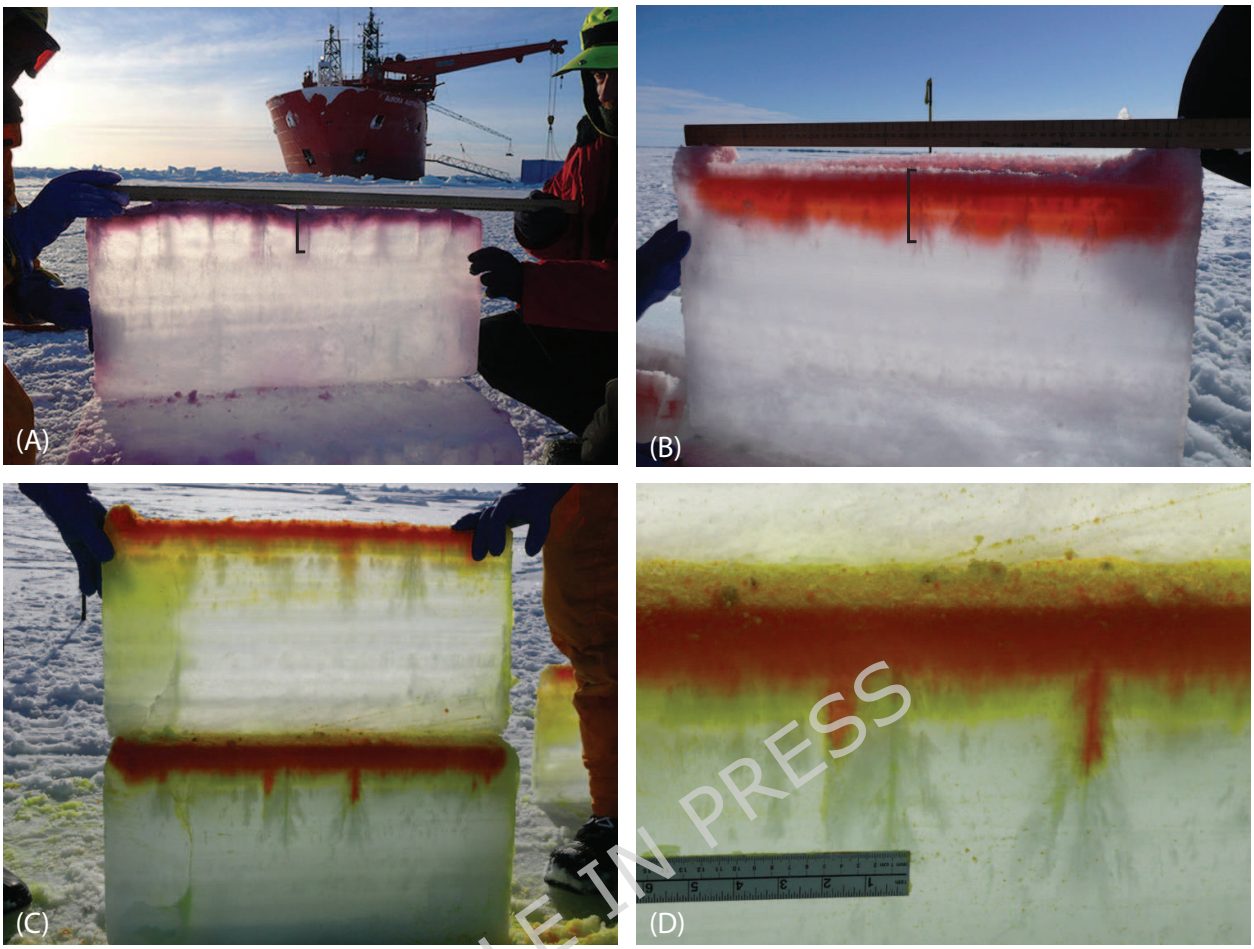

Figure 3: Tracer experiments from SIPEX I. The fluid penetrated about 5 cm into the ice in **(A)** (adapted from [23]), about 10 cm in **(B)**, and about 9 cm in **(C)** and **(D)**. The scale bars in **(A)** and **(B)** each represent 10 cm. In each case the descending fluid passed through an initial layer a few centimeters deep of highly permeable ice of average brine volume fraction in the range 18.5% - 21.5%, until reaching relatively impermeable ice with brine volume fraction of about 10%, where it stopped flowing. In **(A)**, the temperature and brine volume decreased more rapidly, and the tracer stopped after 5 cm. In **(B)** and **(C)** the 10% brine volume threshold was located about 10 cm down, and in **(D)** a tracer plume was also able to descend deeper through a large brine channel.

Percolation Theory Results

Using the crystallographic cores taken at each site, we can match the vertical permeability measurement to ice type based on depth. The details of this process are found in Methods. In Figure 2 (A) we display the granular permeability data along with the curve in equation (1). In Figure 2 (B) we show the percolation theory prediction in logarithmic variables, along with a statistical best fit to the data that shows close agreement to the percolation theory curve. There is a clear surge in permeability values for brine volume fractions above 10%, while the ice is effectively impermeable to bulk flow below the threshold. When plotting the data on a logarithmic scale, it appears that for brine volume fractions above 10% percolation theory accurately captures the data. Indeed, a statistical best fit of the data produces the line $y = 1.97x + 17.5$ while percolation theory yields $y = 2x + 17.5$.

3 Discussion

Granular ice is a significant component of the Antarctic ice pack, and is an increasingly important part of the Arctic sea ice cover. Fluid flow through sea ice governs a broad range of physical and biological processes in the polar marine environment which must be accurately accounted for to improve predictive models. While the critical brine volume fraction for fluid flow in columnar sea ice is about 5%, here we present the first extensive set of *in situ* measurements of the fluid permeability of granular ice. We find its critical brine volume fraction to be about 10%, almost double that for columnar ice. Furthermore, we show the results of tracer experiments in Antarctic sea ice that again support the finding that the critical threshold in granular ice is around 10%. The tracer experiments were conducted during the SIPEX I expedition of September−October 2007 off the coast of East Antarctica between 115° E and 130° E, and 64° S and 66° S [39, 49].

We remark that a more basic version of the permeability measurements presented here for granular ice were first attempted on SIPEX I in 2007. However, at that time we were unable to regularly co-locate or correlate the fluid measurements with the cores taken for crystallographic analysis, as we have rigorously taken care of here. Before SIPEX II in 2012, our experimental techniques were developed and refined on sea ice in McMurdo Sound about 20 km from Scott Base in November and December of 2010, and in the Arctic in spring of 2011 and 2012 [50]. One notable refinement used here was our adaptation of pressure transducers used in reservoir monitoring to record the water level with time in the hole left from partial coring.

An elementary analysis of the compressed powder model [37, 35] confirms that granular microstructures should display higher thresholds than columnar ice. We note that fine-grained columnar ice, which can display geometric similarity to some granular ice, can also exhibit these higher percolation threshold values, while coarse-grained microstructures in granular ice (with higher R_i/R_b ratios) can have lower thresholds similar to columnar ice. By measuring the relative dimensions of the ice grains and the fluid films surrounding them in photomicrographs of granular sea ice, we obtain a model prediction of the percolation threshold for Antarctic granular ice of around 10%, with the possibility of even higher thresholds for more finely grained microstructures. We note, however, that the compressed powder model is an overly simplified idealization of the porous microstructure of sea ice and is limited in its predictive capabilities, with other microstructural features playing a role in fluid transport properties. It should be viewed as a guide for understanding the basic properties of percolation in these types of media, but certainly has limitations and is best used in conjunction with actual fluid permeability measurements, as we do here.

We remark that the higher value for granular ice in comparison to columnar ice is reasonable from a geometrical perspective, particularly in view of Figures 1 and 4. Connectivity and flow can be achieved in columnar ice along the extended brine filaments sandwiched between ice platelets, with low overall porosity, as shown in Figure 4. In granular ice, though, the required porosity must be higher in order to overcome the inherently less interconnected brine microstructure [31], and the more random, labyrinthine fluid pathways that are apparent in the granular ice in Figure 1.

In addition to determining the value of the percolation threshold for granular ice, we also predict the dependence of the vertical fluid permeability on brine volume fraction for ϕ above $\phi_c \approx 10\%$ using percolation theory. A comprehensive theory for the vertical fluid permeability of columnar sea ice was developed, and validated experimentally with laboratory and Arctic field data in [28]. Microscale imaging methods based on X-ray computed tomography (CT) and pore structure analysis were also developed to provide detailed pictures of the brine microstructure and the evolution of its connectivity with temperature [28, 51].

We demonstrate that the value of the percolation threshold changes significantly with changes in polycrystalline microstructure. This is typical in percolation theory, where the threshold value for

the two dimensional square lattice, for example, is quite different than for the hexagonal lattice [34]. Nevertheless, the fluid permeability critical exponent that characterizes the increase in permeability above the threshold is believed to be *universal* for lattices, depending only on dimension and not on the details of the lattice [34]. Somewhat surprisingly, we found in [28] that the fluid permeability critical exponent for columnar ice is the same as the universal *lattice* value in three dimensions. We find here that percolation theory [52, 12, 28] and data on pore size distributions [31] allow us to predict that the critical exponent for permeability above ϕ_c for granular ice should be the same as the universal lattice value that holds for columnar ice. This is indeed what we find in the data, in what appears to be a notable demonstration of universality for a complex random medium in the continuum. Our findings here add further weight to the vision put forth in [53] that statistical physics provides a natural, powerful framework for formulating and addressing key questions in the physics of sea ice.

This work demonstrates the applicability of percolation theory to fluid flow through sea ice for ice types other than columnar ice. It also demonstrates that considering the microstructure of the ice is vital when modeling any process in which fluid flow through the ice is relevant, such as nutrient replenishment, biological colonization, gas exchange, and melt pond evolution. Our findings also allow for a better understanding of previous experimental results showing lower brine channel densities and delayed brine channel initiation in granular ice compared to columnar ice, with critical Rayleigh numbers for convection being controlled by ice permeability [54]. We note also that the conclusions in [31] invalidated the earlier intuitive belief in [54] that a lower density of brine channels for experimental granular ice compared to columnar ice, at a given growth rate, resulted from "reduced geometrical constraints enhancing the efficiency of individual brine channels in granular ice, and therefore reducing brine channel density."

We reiterate that the percolation threshold of approximately 10% for bulk fluid flow through granular sea ice has been observed in field experiments involving flow over scales of at least several centimeters, as indicated in Figure 3 and in our hydrological bail tests. Our findings, however, do not preclude fluid activity over shorter ranges within small-scale connected brine structures, even for brine volume fractions below 10%. Local fluxes on these smaller scales are particularly important for microbial life that can inhabit the brine inclusions. In percolation theory [33, 34], a porosity or volume fraction above the threshold signals that there is bulk transport across a very large (or infinite) sample, yet at the same time this does not preclude the existence of open clusters which can be connected over relatively large scales − even for porosites well below the threshold. We also remark that sea ice is a highly inhomogeneous porous composite, with large variations in the brine microstructure and fluid transport properties that can occur over distances of just a few centimeters. Here again as a result, measurements of fluid flow in sea ice could potentially yield unusually large values even for porosities below 10%, for example, if a brine channel was active during the measurement process. We note that our results apply to the region off the coast of East Antarctica where the experiments were conducted. While it is reasonable to assume that the threshold applies to granular sea ice in other geographic areas, confirming this claim requires further field experimentation in different regions.

Our results strongly support the finding that the critical threshold for bulk vertical flow through granular sea ice off the coast of East Antarctica is about 10%. We have already pointed out uncertainties in the results such as the over-simplification of the compressed powder model. But we have also assumed that bubbles are not playing a role in the findings. However, particularly if bubbles are connected and form larger open pore spaces, then they could play a role in the fluid transport properties, and in the observed critical threshold, presumably making it easier for fluid to flow. In the measurements of fluid permeability, we use tight fitting pipes coated with foam to block out the horizontal flow, but there may be some seepage. Also, there are uncertainties

inherent in correlating the temperature and salinity, and therefore brine volume fraction, at the bottom of a partial core, with the permeability measurements there. Finally, as noted before, the tracer experiments were quite rudimentary, and not originally designed to measure the critical porosity for fluid flow. While they did support the 10% finding, nevertheless significant uncertainties remain, such as what really stopped the downward tracer flow, did the fluid freeze, how fast did the fluid move, and so on. Conducting such tracer experiments again, while addressing these issues and doing a more careful crystallographic analysis would potentially yield interesting results about fluid transport through sea ice.

All of the above mentioned physical and biological processes depend critically on fluid flow through the ice and are important factors in understanding the polar marine environment. We have shown that the percolation threshold for sea ice, especially in the Antarctic ice pack, cannot be assumed to be 5% homogeneously. In order to facilitate accuracy in models for both small-scale processes and large-scale behavior, it is imperative that granular sea ice be considered separately from columnar sea ice to determine the characteristics and behavior of the pack as a whole.

4 Methods

Percolation Theory

Percolation theory can be used to model transport in disordered materials where the connectedness of one phase, like brine in sea ice, dominates the effective behavior [33, 34] Consider the square ($d = 2$) or cubic ($d = 3$) network of bonds joining nearest neighbor sites on the integer lattice $\mathbb{Z}^d$. The bonds are assigned fluid permeabilities $k_0 > 0$ (open) or $k_0 = 0$ (closed) with probabilities p and $1 - p$, respectively. The percolation threshold is the critical probability p_c, $0 < p_c < 1$, where an infinite, connected set of open bonds first appears as p increases. In $d = 2$, $p_c = \frac{1}{2}$, and in $d = 3$, $p_c \approx \frac{1}{4}$. Let $k(p)$ be the permeability of this random network in the vertical direction. Below the percolation threshold ($p < p_c$), $k(p) = 0$. For $p > p_c$ and near the threshold, $k(p)$ exhibits power law behavior, $k(p) \sim k_0(p - p_c)^e$ as $p \to p_c^+$, where e is the permeability critical exponent. For lattice models, critical exponents are believed to be *universal*, depending only on the dimension d. In the lattice case, we also note that e is equal to the lattice electrical conductivity exponent t [52, 34, 55, 56]. For $d = 3$, there is a rigorous bound (for a model of the percolating backbone) that $1 \leq t \leq 2$ [55], and it is believed that $t \approx 2.0$ [34].

Although e can take non-universal values in the continuum, it was shown [52, 56, 34] that for lognormally distributed inclusions as in [41], e takes the universal lattice value with $e \approx 2$. We found this to be the case for columnar ice in [28] and here for granular ice [31]. The scaling factor k_0 was estimated in [28] using critical path analysis and X-ray CT observations of throat sizes, that is, the sizes of the "bottlenecks" within the connected brine pathways, or the largest radius of a sphere that can fit anywhere along the brine pathway, or be inscribed within it. Here we use the same k_0 value for granular ice, since the throat sizes found in [31] correlate well with the parameters used in [28], so that above the threshold,

$$k(\phi) \sim 3\,(\phi - \phi_c)^2 \times 10^{-8}\ \mathrm{m}^2, \quad \phi \to \phi_c^+, \tag{1}$$

with critical brine volume fraction $\phi_c \approx 0.1$ for granular ice, as we see below.

Compressed Powder Model

To theoretically estimate the percolation threshold ϕ_c for fluid transport in Antarctic granular ice, we use the compressed powder model [35, 36, 37]. It was useful in originally explaining why ϕ_c for

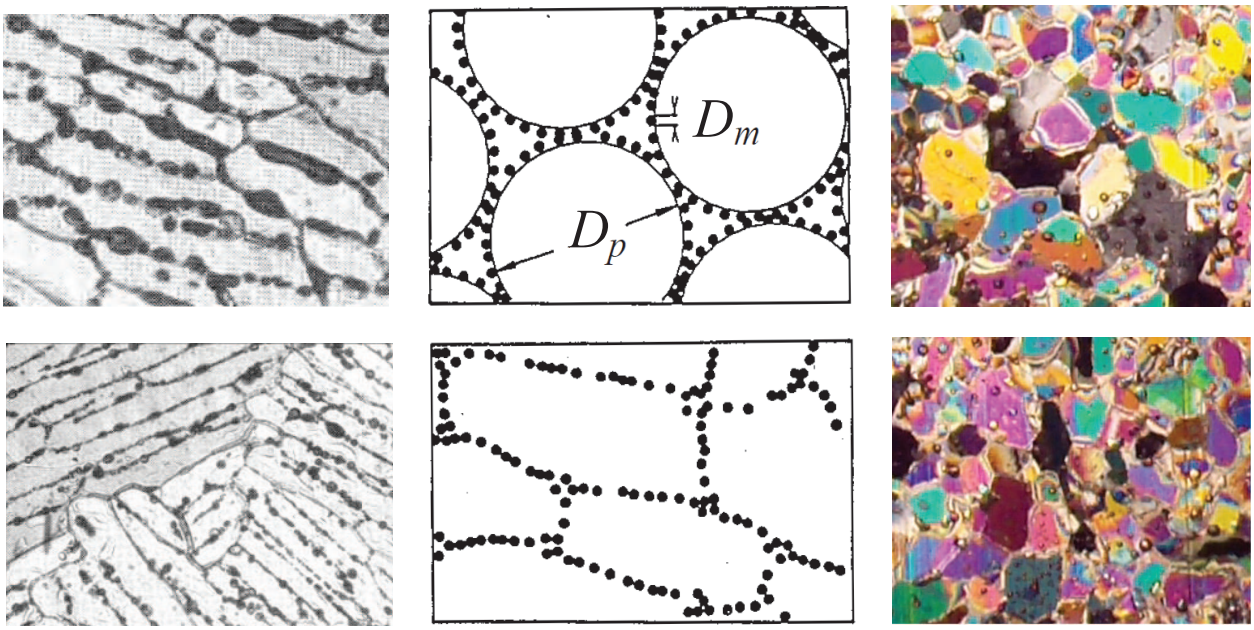

Figure 4: Columnar and granular polycrystalline microstructures, and the compressed powder model. Left column: microstructure of columnar sea ice – aligned ice platelets with brine inclusions in between [57, 27]; Middle column: compressed powder model [35, 36, 37] used to predict percolation thresholds for powder composites as a function of the ratio of particle sizes; Right column: crystalline microstructure of granular sea ice from the Bellingshausen Sea, with brine films between the ice grains. The grains have statistically isotropic orientations, as indicated by the colorations shown.

columnar ice had a value that was so much lower than for classical lattice models, and in predicting that it should be around 5% [27]. This model is perhaps even more applicable to granular ice with crystals that are more spherically-shaped, so that the degree of compression in the compressed powder model is minimal, as indicated in Figure 4.

In the compressed powder model, large polymer spheres of radius R_p and diameter $D_p = 2R_p$ are mixed with much smaller metal spheres of radius R_m and diameter $D_m = 2R_m$, and the mixture is compressed. The main parameter controlling the threshold is the ratio $\xi = R_p/R_m$. An approximate formula for the critical volume fraction for percolation of the small metal spheres is given by $\phi_c = (1 + \xi\theta/(4X_c))^{-1}$, where θ is a reciprocal planar packing factor, the ratio of total planar area to the area occupied by particles, and X_c is the critical surface area fraction of the larger particles which must be covered by the smaller particles for percolation to occur. Based on microstructural analysis, values of $X_c = 0.42$ and $\theta = 1.27$ agree with empirical experimentation [37]. This mixture geometry is roughly similar to the ice-brine microstructure of sea ice, where the ice grains or platelets have "diameter" or length $D_i = 2R_i$ in the long dimension (analogous to D_p in the compressed powder before compression), and the brine inclusions (or tubes) have "diameter" $D_b = 2R_b$, or the thickness of a brine film around an ice grain in the granular case, with $\xi = R_i/R_b$ in this case. We have estimated a range of ξ values from photomicrographs of granular microstructures, as in Figure 4, and obtained a representative, average value of around $\xi \approx 12$, leading to a threshold value of around $\phi_c \approx 10\%$. By comparison, a range of ξ values obtained for the columnar ice on the left in Figure 4 gave a representative average of about $\xi \approx 24$, and a threshold value of around $\phi_c \approx 5\%$ [27]. In Figure 5, we illustrate the relationship between

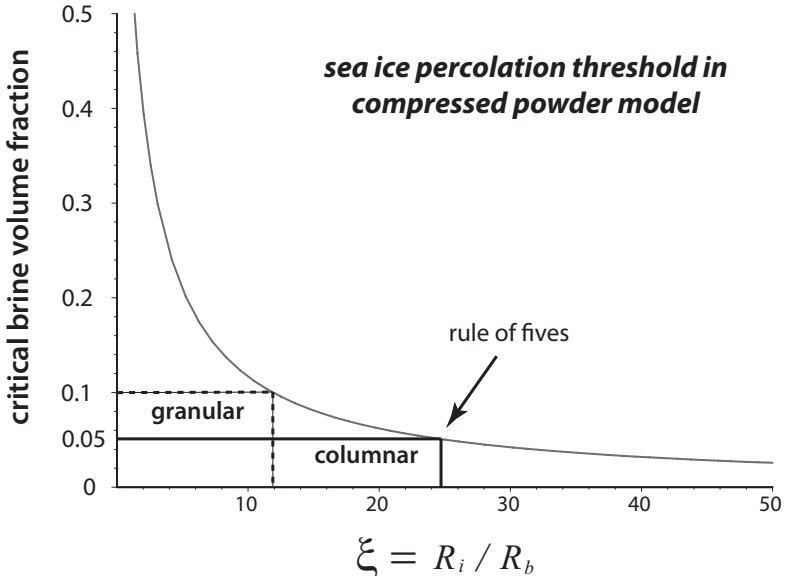

Figure 5: The percolation threshold in the compressed powder model is shown as a function of the ratio of the particle radii.

ξ and critical brine volume fraction, highlighting the two points on the curve corresponding to our findings for granular and columnar ice, respectively.

Fluid Permeability Data

The *in situ* permeability data were collected using a hydrologic bail test [58] where partial cylindrical holes were drilled vertically into the sea ice and the cores removed. Then a tight-fitting plastic pipe wrapped in foam (a packer) was inserted into the partial hole to block any horizontal inflow from the exposed surfaces. A pressure transducer (in a frame to keep it vertical) was then placed at the bottom of the hole to measure the height $h(t)$ in meters of the rising water column as a function of time t in seconds. Temperature and salinity measurements were taken from the bottom 2 cm of each partial core, allowing us to identify the brine volume fraction at the interface. While the corer has "core catchers" at its bottom to keep the ice core inside the corer as it's lifted out, they often did not work, so we developed a *lasso* method of extracting a partial core. Using a thin enough rope to fit between the ice core and the surrounding ice, we tied a lasso around the top of the core. While pulling up tightly on the lasso, we simultaneously jammed a carefully sized bamboo pole down between the partial core and the surrounding ice. One quick downward thrust usually broke the partial core off at the bottom of the hole, leaving a flat ice surface at the bottom for our transducer frame to sit properly.

The permeability of the ice just underneath the borehole can be accurately estimated using the equation

$$h(t) = h(t_0)e^{-k_{exp}t(g\rho/\eta L)}, \tag{2}$$

with measured permeability k_{exp} (m^2), ice thickness beneath the borehole L (m), density ρ ($\mathrm{kg\,m^{-3}}$), gravitational constant g ($\mathrm{m\,s^{-2}}$), and initial time t_0. The vertical component k_v of the permeability can then be found using the calculations in [58], which are based on simulations of the pressure field in the ice and have been verified by measurement. For sea ice, like that of Arctic columnar ice, with a ratio of lateral permeability to vertical permeability $k_l/k_v \approx 0.1$, the vertical component

can be calculated with:

$$k_v = \frac{k_{exp}}{0.17 + 10.7\mathrm{m}^{-1}L}\,. \tag{3}$$

For granular sea ice, with a far more isotropic crystallographic and pore structure, as shown in Figure 1, the vertical component of the permeability may be calculated using:

$$k_v = \frac{k_{exp}}{0.15 + 32.4\mathrm{m}^{-1}L}\,, \tag{4}$$

which corresponds to the isotropic case where $k_l/k_v \approx 1$, more inline with the microstructure of granular sea ice.

In order to correlate the permeability measurement with the ice type, a full crystallographic core was taken at each measurement site. For best results, we primarily collected core samples from level, undeformed ice. Cores were immediately taken on board the *Aurora Australis*, where a standard crystallographic analysis was conducted in a -20° C freezer using thin sections and cross-polarizing film. We then matched the depths of our permeability measurements to those of the crystallographic core for each site to identify ice type and partition the data by crystal classification. Permeability measurements were kept to within 3 meters of the crystallographic core to ensure close correspondence. Example images of the polycrystalline microstructure of Antarctic ice under cross-polarization are shown in Figure 1. The left panel displays a columnar sample and the right panel a granular one. The samples were collected in October 2007 during the SIMBA expedition [30]. Some granular crystalline microstructures that we observed during SIPEX II were very similar to what is seen on the right in Figure 4.

Theoretical Bounds

Finally, we demonstrate that the empirical data just discussed are captured by known theoretical bounds. We consider low Reynolds number flow of brine with viscosity η through sea ice, and theoretical bounds on sea ice fluid permeability. The volume fractions of brine and ice are ϕ and $1-\phi$, respectively, where the effects of small air bubbles, typically isolated from one another, are assumed to be negligible. The velocity and pressure fields in the brine satisfy the Stokes' equations for incompressible fluids. Under appropriate assumptions [34], the homogenized velocity $\mathbf{v}(\mathbf{x})$ and pressure $p(\mathbf{x})$ satisfy Darcy's law and the incompressibility condition for velocity,

$$\mathbf{v} = -\frac{1}{\eta}\,\mathbf{k}\,\nabla p \quad \text{and} \quad \nabla\cdot\mathbf{v} = 0. \tag{5}$$

In (5), $\mathbf{k}$ is the permeability tensor with vertical permeability $\mathrm{k}_{\mathbf{z}} = k$, which has units of m^2.

In previous work [59, 28] rigorous upper bounds for the vertical fluid permeability $k(\phi)$ of sea ice were found, based on an observed lognormal distribution for the horizontal cross-sectional areas $A(\phi)$ of the brine inclusions [41]. In this case $Z = \ln A$ has a normal probability density with mean μ and variance σ^2,

$$P(Z) = \frac{1}{\sqrt{2\pi\sigma^2}}\; e^{-(Z-\mu)^2/2\sigma^2}. \tag{6}$$

The cross-sectional radius $a(\phi) = 7\times10^{-5} + (1.6\times10^{-4})\phi$ (m) increases according to measurements of pore sizes with temperature and is given in [60, 41]. In [31] the statistical behavior of the pores in granular ice was found to be similar to that in [41], so that these parameters and bounds are applicable to our granular ice permeability data. The bound is a special case of optimal void bounds [34, 61], and takes the form

$$k(\phi) \le \frac{\phi}{8\pi}\,\langle A(\phi)\rangle\; e^{\sigma^2} \tag{7}$$

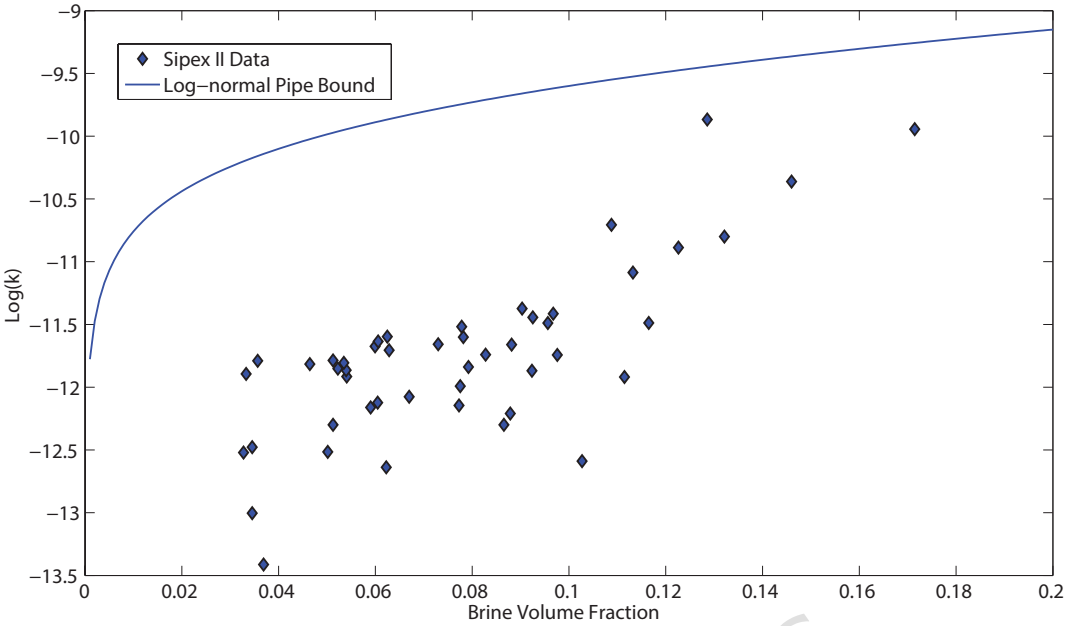

Figure 6: A comparison of *in situ* data from SIPEX II on the vertical fluid permeability k (m^2) of Antarctic granular ice with a rigorous upper bound.

with variance $\sigma^2 \approx 1$ and $\langle A(\phi) \rangle = \pi a^2(\phi)$ as in [41]. The *lognormal pipe bound* in (7) captures all our data for granular ice, as shown in Figure 6.

Acknowledgments. We thank the crew of the *Aurora Australis* and participants of SIPEX I and SIPEX II for their help in obtaining the data presented here. In particular, we thank Ian Allison and Tony Worby for their leadership of SIPEX I and SIPEX II, respectively. We also thank the University of Tasmania, the Australian Antarctic Division, and the ACE Cooperative Research Centre for their support. Finally, we are most grateful to David Lubbers for his immeasurable contributions to this work and to the success of the expeditions in which he participated.

Funding Statement. We gratefully acknowledge support from the Division of Mathematical Sciences and Arctic Natural Sciences at the US National Science Foundation (NSF) through grants DMS-0940249, ARC-0934721, DMS-1413454, DMS-2136198, and DMS-2206171. We are also grateful for support from the Applied and Computational Analysis Program and the Arctic and Global Prediction Program at the US Office of Naval Research through grants N00014-13-1-0291, N00014-18-1-2552, N00014-18-1-2041, N00014-21-1-2909 and N00014-26-1-2114. J. L. Tison acknowledges the support of the Belgian Science Policy (contract SD/CA/03A) and of the Belgian FRS-FNRS (Fons National de la Recherche Scientifique - FRFC contract no. 2.4649.07).

Data Availability. The datasets analyzed during the current study are available in the SIPEX_II repository at `https://data.aad.gov.au/metadata/SIPEX_II`.

Author Contributions. KMG, CMF, AG, JL, and CS conceived and designed the experiments. KMG, AG, CS, and JLT performed the experiments. All authors analyzed the data. KMG, CMF,

AG, JL, CS, and JLT contributed materials and analysis tools. KMG, AG, DQM, and CS wrote the main manuscript text. All authors reviewed the manuscript.

References

[1] D. N. Thomas, editor. *Sea Ice, 3rd Edition.* John Wiley & Sons, Chichester, UK; Hoboken, NJ, 2017.

[2] W. F. Weeks and S. F. Ackley. The growth, structure and properties of sea ice. *CRREL Monograph 82-1*, page 130 pp., 1982.

[3] K. R. Arrigo. Sea ice ecosystems. *Annual Review of Marine Science*, 6:439–467, 2014.

[4] J. Stroeve and D. Notz. Changing state of Arctic sea ice across all seasons. *Environmental Research Letters*, 13(10):103001, 2018.

[5] Q. Shu, Q. Wang, Z. Song, F. Qiao, J. Zhao, M. Chu, and X. Li. Assessment of sea ice extent in CMIP6 with comparison to observations and CMIP5. *Geophysical Research Letters*, 47(9):e2020GL087965, 2020.

[6] W. N. Meier and J. Stroeve. An updated assessment of the changing Arctic sea ice cover. *Oceanography*, 35(3/4):10–19, 2022.

[7] A. Purich and E. W. Doddridge. Record low Antarctic sea ice coverage indicates a new sea ice state. *Communications Earth & Environment*, 4(314):9 pp., 2023.

[8] W. Hobbs, P. Spence, A. Meyer, S. Schroeter, A. D. Fraser, P. Reid, T. R. Tian, Z. Wang, G. Liniger, E. W. Doddridge, and P. W. Boyd. Observational evidence for a regime shift in summer Antarctic sea ice. *Journal of Climate*, 37(7):2263 – 2275, 2024.

[9] J. Stroeve, M. M. Holland, W. Meier, T. Scambos, and M. Serreze. Arctic sea ice decline: Faster than forecast. *Geophysical Research Letters*, 34(9), 2007.

[10] K. M. Golden, L. G. Bennetts, E. Cherkaev, I. Eisenman, D. Feltham, C. Horvat, E. Hunke, C. Jones, D. Perovich, P. Ponte-Castañeda, C. Strong, D. Sulsky, and A. Wells. Modeling sea ice. *Notices of the American Mathematical Society*, 67(10):1535–1555, 2020.

[11] C. Petrich and H. Eicken. Growth, structure, and properties of sea ice. In D. N. Thomas and G. S. Dieckmann, editors, *Sea Ice*, pages 23–77. Wiley-Blackwell, 2009.

[12] K. M. Golden. Climate change and the mathematics of transport in sea ice. *Notices of the American Mathematical Society*, 56:562–584, 2009.

[13] A. Gully, J. Lin, E. Cherkaev, and K. M. Golden. Bounds on the complex permittivity of polycrystalline composites by analytic continuation. *Proceedings of the Royal Society A*, 471(2174):20140702, 2015.

[14] H. Eicken, T. C. Grenfell, D. K. Perovich, J. A. Richter-Menge, and K. Frey. Hydraulic controls of summer Arctic pack ice albedo. *Journal of Geophysical Research (Oceans)*, 109(C18):C08007.1–C08007.12, 2004.

[15] C. Polashenski, K. M. Golden, D. K. Perovich, E. Skyllingstad, A. Arnsten, C. Stwertka, and N. Wright. Percolation blockage: A process that enables melt pond formation on first year Arctic sea ice. *Journal of Geophysical Research (Oceans)*, 122(1):413–440, 2017.

[16] T. Maksym and M. O. Jeffries. A one-dimensional percolation model of flooding and snow ice formation on Antarctic sea ice. *Journal of Geophysical Research*, 105(C11):26313–26331, 2000.

[17] I. Merkouriadi, G. E. Liston, R. M. Graham, and M. A. Granskog. Quantifying the potential for snow-ice formation in the Arctic Ocean. *Geophysical Research Letters*, 47:e2019GL08502, 2019.

[18] B. Delille, M. Vancoppenolle, N.-X. Geilfus, B. Tilbrook, D. Lannuzel, V. Schoemann, S. Becquevort, G. Carnat, D. Delille, C. Lancelot, L. Chou, G. S. Dieckmann, and J.-L. Tison. Southern Ocean CO_2 sink: The contribution of the sea ice. *Journal of Geophysical Research: Oceans*, 119(9):6340–6355, 2014.

[19] G. Carnat, F. Brabant, I. Dumont, M. Vancoppenolle, S. Ackley, C. Fritsen, B. Delille, and J.-L. Tison. Influence of short-term synoptic events and snow depth on DMS, DMSP, and DMSO dynamics in Antarctic spring sea ice. *Elementa: Science of the Anthropocene*, 4, 2016.

[20] J.-L. Tison, B. Delille, and S. Papadimitriou. Gases in sea ice. In David N Thomas, editor, *Sea Ice, 3rd Edition*, pages 433–471. John Wiley & Sons, Chichester, UK; Hoboken, NJ, 2017.

[21] V. I. Lytle and S. F. Ackley. Heat flux through sea ice in the Western Weddell Sea: Convective and conductive transfer processes. *Journal of Geophysical Research*, 101(C4):8853–8868, 1996.

[22] H. J. Trodahl, M. J. McGuiness, P. J. Langhorne, K. Collins, A. E. Pantoja, I. J. Smith, and T. G. Haskell. Heat transport in McMurdo Sound first-year fast ice. *Journal of Geophysical Research*, 105(C5):11347–11358, 2000.

[23] N. Kraitzman, R. Hardenbrook, H. Dinh, N. B. Murphy, E. Cherkaev, J. Zhu, and K. M. Golden. Homogenization for convection-enhanced thermal transport in sea ice. *Proceedings of the Royal Society A*, 480(2296):22 pp. and issue cover, 2024.

[24] H. Eicken. The role of sea ice in structuring Antarctic ecosystems. *Polar Biology*, 12:3–13, 1992.

[25] C. H. Fritsen, V. I. Lytle, S. F. Ackley, and C. W. Sullivan. Autumn bloom of Antarctic pack-ice algae. *Science*, 266:782–784, 1994.

[26] S.F. Ackley and C.W. Sullivan. Physical controls on the development and characteristics of Antarctic sea ice biological communities— a review and synthesis. *Deep Sea Research Part I: Oceanographic Research Papers*, 41(10):1583–1604, 1994.

[27] K. M. Golden, S. F. Ackley, and V. I. Lytle. The percolation phase transition in sea ice. *Science*, 282:2238–2241, 1998.

[28] K. M. Golden, H. Eicken, A. L. Heaton, J. Miner, D. Pringle, and J. Zhu. Thermal evolution of permeability and microstructure in sea ice. *Geophysical Research Letters*, 34:L16501, 2007.

[29] G. Frankenstein and R. Garner. Equations for determing the brine volume of sea ice from -0.5^o to -22.9^o C. *Journal of Glaciology*, 6(48):943–944, 1967.

[30] M. J. Lewis, J. L. Tison, B. Weissling, B. Delille, S. F. Ackley, F. Brabant, and H. Xie. Sea ice and snow cover characteristics during the winter–spring transition in the Bellingshausen Sea: An overview of SIMBA 2007. *Deep Sea Research Part II: Topical Studies in Oceanography*, 58(9):1019–1038, 2011.

[31] M. Oggier and H. Eicken. Seasonal evolution of granular and columnar sea ice pore microstructure and pore network connectivity. *Journal of Glaciology*, 68(271):833–848, 2022.

[32] K. M. Meiners, K. M. Golden, P. Heil, J. L. Lieser, R. Massom, B. Meyer, and G. D. Williams. Introduction: SIPEX-2: A study of sea-ice physical, biogeochemical and ecosystem processes off East Antarctica during spring 2012. *Deep Sea Research Part II: Topical Studies in Oceanography*, 131:1–6, 2016.

[33] D. Stauffer and A. Aharony. *Introduction to Percolation Theory, Second Edition*. Taylor and Francis Ltd., London, 1992.

[34] S. Torquato. *Random Heterogeneous Materials: Microstructure and Macroscopic Properties*. Springer-Verlag, New York, 2002.

[35] R. P. Kusy and D. T. Turner. Electrical resistivity of a polymeric insulator containing segregated metallic particles. *Nature*, 229:58–59, 1971.

[36] A. Malliaris and D. T. Turner. Influence of particle size on the electrical resistivity of compacted mixtures of polymeric and metallic powders. *J. Appl. Phys.*, 42(2):614–618, 1971.

[37] R. P. Kusy. Influence of particle size ratio on the continuity of aggregates. *Journal of Applied Physics*, 48(12):5301–5303, 1977.

[38] A Priou. *Dielectric Properties of Heterogeneous Materials*. Elsevier, 1992.

[39] A. P. Worby, A. Steer, J. L. Lieser, P. Heil, D. Yi, T. Markus, I. Allison, R. A. Massom, N. Galin, and J. Zwally. Regional-scale sea-ice and snow thickness distributions from in situ and satellite measurements over East Antarctica during SIPEX 2007. *Deep Sea Research Part II: Topical Studies in Oceanography*, 58(9-10):1125–1136, 2011.

[40] B. Light, G. A. Maykut, and T. C. Grenfell. Effects of temperature on the microstructure of first-year Arctic sea ice. *Journal of Geophysical Research*, 108(C2):3051, 2003.

[41] D. K. Perovich and A. J. Gow. A quantitative description of sea ice inclusions. *Journal of Geophysical Research*, 101(C8):18,327–18,343, 1996.

[42] D. K. Perovich, T. C. Grenfell, B. Light, B. C. Elder, J. Harbeck, C. Polashenski, W. B. Tucker III, and C. Stelmach. Transpolar observations of the morphological properties of Arctic sea ice. *Journal of Geophysical Research*, 114:C00A04, 2009.

[43] Y. Liu, J. R. Key, X. Wang, and M. Tschudi. Multidecadal Arctic sea ice thickness and volume derived from ice age. *Cryosphere*, 14(4):1325–1345, 2020.

[44] W. B. Tucker III, A. J. Gow, D. A. Meese, H. W. Bosworth, and E. Reimnitz. Physical characteristics of summer sea ice across the Arctic Ocean. *Journal of Geophysical Research*, 104:1489–1504, 1999.

[45] H. Eicken. Deriving modes and rates of ice growth in the Weddell Sea from microstructural, salinity and stable-isotope data. In *Antarctic Sea Ice: Physical Processes, Interactions and Variability*, pages 89–122. American Geophysical Union, 1998.

[46] A. P. Worby and R. Massom. *The Structure and Properties of Sea Ice and Snow Cover in East Antarctic Pack Ices*. Antarctic CRC Report, Hobart, Australia, 1995.

[47] T. Maksym and T. Markus. Antarctic sea ice thickness and snow-to-ice conversion from atmospheric reanalysis and passive microwave snow depth. *Journal of Geophysical Research*, 113:C02S12, 2008.

[48] K. M. Meiners. Parent metadata record for all metadata created from the SIPEX II voyage of the Aurora Australis, 2012-2013 season - Sea Ice Physics and Ecosystem eXperiment (Version 1) [Dataset]. *Australian Antarctic Data Centre*, 2014.

[49] C. Sampson, K. M. Golden, A. Gully, and A. P. Worby. Surface impedance tomography for Antarctic sea ice. *Deep Sea Research Part II: Topical Studies in Oceanography*, 58(9-10):1149–1157, 2011.

[50] W. Pyper. The Golden Rule of Sea Ice Permeability. *Australian Antarctic Magazine*, (24):12 – 14, June 2013.

[51] D. J. Pringle, J. E. Miner, H. Eicken, and K. M. Golden. Pore-space percolation in sea ice single crystals. *Journal of Geophysical Research (Oceans)*, 114:C12017, 12 pp., 2009.

[52] B. Berkowitz and I. Balberg. Percolation approach to the problem of hydraulic conductivity in porous media. *Transport in Porous Media*, 9:275–286, 1992.

[53] A. F. Banwell, J. C. Burton, C. Cenedese, K. M. Golden, and J. Åström. Physics of the cryosphere. *Nature Reviews Physics*, 5(8):446–449, 2023.

[54] J.-L. Tison and V. Verbeke. Chlorinity/salinity distribution patterns in experimental granular sea ice. *Annals of Glaciology*, 33:13–19, 2001.

[55] K. M. Golden. Convexity and exponent inequalities for conduction near percolation. *Physical Review Letters*, 65(24):2923–2926, 1990.

[56] B. I. Halperin, S. Feng, and P. N. Sen. Differences between lattice and continuum percolation transport exponents. *Physical Review Letters*, 54(22):2391–2394, 1985.

[57] S. A. Arcone, A. J Gow, and S. McGrew. Structure and dielectric properties at 4.8 and 9.5 GHz of saline ice. *J. Geophys. Res.*, 91(C12):14281–14303, 1986.

[58] J. Freitag and H. Eicken. Meltwater circulation and permeability of Arctic summer sea ice derived from hydrological field experiments. *Journal of Glaciology*, 49:349–358, 2003.

[59] K. M. Golden, A. L. Heaton, H. Eicken, and V. I. Lytle. Void bounds for fluid transport in sea ice. *Mechanics of Materials*, 38:801–817, 2006.

[60] C. Bock and H. Eicken. A magnetic resonance study of temperature-dependent microstructural evolution and self-diffusion of water in Arctic first-year sea ice. *Annals of Glaciology*, 40:179–184, 2005.

[61] S. Torquato and D. C. Pham. Optimal bounds on the trapping constant and permeability of porous media. *Physical Review Letters*, 92:255505:1–4, 2004.